

Photoelectron spectroscopy of CN^- , NCO^- , and NCS^-

Stephen E. Bradforth, Eun Ha Kim, Don W. Arnold,^{a)} and Daniel M. Neumark^{b)}
Department of Chemistry, University of California, Berkeley, California 94720

(Received 8 September 1992; accepted 2 October 1992)

The 266 nm photoelectron spectra of CN^- , NCO^- , and NCS^- have been recorded with a pulsed time-of-flight photoelectron spectrometer. The photoelectron spectrum of CN^- has also been recorded at 213 nm revealing transitions to the $A^2\Pi$ state as well as the ground $X^2\Sigma^+$ state of the CN radical. The following adiabatic electron affinities (EAs) are determined: $\text{EA}(\text{CN}) = 3.862 \pm 0.004$ eV, $\text{EA}(\text{NCO}) = 3.609 \pm 0.005$ eV, and $\text{EA}(\text{NCS}) = 3.537 \pm 0.005$ eV. The adiabatic electron affinity of cyanide is in disagreement with the currently accepted literature value. Our measurement of the electron affinity of NCS confirms recent theoretical estimates that dispute the literature experimental value. By Franck–Condon analysis of the vibrational progressions observed in each spectrum, the change in bond lengths between anion and neutral are also determined. For NCO^- this yields $R_0(\text{C–N}) = 1.17 \pm 0.01$ Å and $R_0(\text{C–O}) = 1.26 \pm 0.01$ Å, and for CN^- the equilibrium bond length is found to be $R_e(\text{C–N}) = 1.177 \pm 0.004$ Å. The gas phase fundamental for CN^- is determined for the first time: $\nu = 2035 \pm 40$ cm^{-1} .

I. INTRODUCTION

The CN^- , NCO^- , and NCS^- anions are of considerable interest in both solution phase and gas phase chemistry. The three anions are “pseudohalides” in that they are closed shell species with relatively high electron binding energies. On the other hand, there are important chemical differences in comparison to the halide ions; in transition metal complexes, for example, the halide and cyanide anions are at opposite ends of the spectrochemical series. A number of experimental and theoretical studies of the spectroscopy and thermochemistry of these anions have been performed in recent years. However, several quantities, particularly the electron affinities of the NCO and NCS radicals, are not well determined. In order to address this, we have measured the ultraviolet photoelectron spectra of the three anions. The spectra yield accurate values of the radical electron affinities, as well as some anion vibrational frequencies and bond lengths.

The spectroscopy of the CN radical has been thoroughly studied,¹ but, while CN^- has been investigated in various condensed phase environments,^{2–5} CN^- has not been fully characterized in the gas phase. Neither the bond length nor the vibrational frequency for gas phase CN^- have been experimentally determined, although there has been very high quality *ab initio* theory performed to describe the ion.^{6,7} The CN electron affinity (EA) has been measured by Leone and co-workers,⁸ whose value of 3.821 ± 0.004 was in good agreement with the previous experimental measurement of Berkowitz (3.82 ± 0.02 eV).⁹ CN^- has a higher reported electron binding energy than any atomic or other diatomic species, and is therefore a desirable calibration standard for our photoelectron spectrometer. However, our photoelectron spectra show the CN electron affinity to be slightly but significantly higher than the currently accepted value of Leone. In addition, we ob-

serve a “hot band” from vibrationally excited CN^- , yielding the gas phase vibrational frequency, and we obtain the CN^- bond length from a Franck–Condon analysis.

Despite the well characterized spectroscopy of the radicals NCO and NCS,¹⁰ the electron affinities for these species have not been accurately determined; currently the EA's listed in the compilation of Lias *et al.*¹¹ are 3.59 ± 0.36 and 2.15 ± 0.02 eV for NCO and NCS respectively. The value for the electron affinity of NCS, obtained from Page's magnetron experiments,¹² is particularly suspect. Not only does it seem inconsistent with the other CN containing molecules, it is also considerably lower than theoretical estimates of this quantity.¹³ We note that Page's accompanying result for $\text{EA}(\text{CN})$, 2.80 eV, is similarly too low.¹² Dillard and Franklin derived $\text{EA}(\text{NCS}) = 3.51$ eV from measured heats of formation of NCS and NCS^- in ion molecule reactions,¹⁴ the most recent theoretical work supports this value with a calculated EA of 3.45 eV.¹³ We show that the true electron affinity is close to that derived from the thermochemical cycle and the theoretical value, and that the previous “direct” measurement of the EA is in error.

The vibrational spectroscopy of the NCO^- and NCS^- anions have been thoroughly investigated in various alkali halide matrices.^{15–18} In addition, high resolution infrared gas phase spectroscopy has been performed on both NCO^- and NCS^- in Saykally's laboratory.^{19,20} This work yielded the ν_3 fundamental frequency and the equilibrium rotational constant for each of these linear ions. However, as isotopically substituted spectra were not recorded, the rotational constant does not completely define the molecular structure, and therefore the two bond lengths remain unknown for each ion. In contrast, for the NCO radical at least, ¹⁵N isotopic substitution in the optical spectra, along with microwave data for ¹⁴NCO, yields the individual neutral bond lengths, $R_0(\text{C–N})$ and $R_0(\text{C–O})$.²¹ With this data for the neutral bond lengths, and a Franck–Condon analysis of the NCO^- photoelectron spectrum, we determine the individual bond lengths for the NCO^- anion.

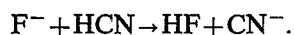
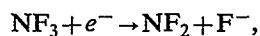
^{a)}NSF Predoctoral Fellow.

^{b)}NSF Presidential Young Investigator and Camille and Henry Dreyfus Teacher–Scholar.

II. EXPERIMENTAL

The photoelectron spectra of NCO^- , NCS^- , and CN^- were recorded on our fixed-frequency negative ion photoelectron spectrometer. This apparatus has been described in detail elsewhere.²² Briefly, the instrument is a dual time-of-flight photoelectron spectrometer. A gas mixture at a stagnation pressure of ca. 3 atm is expanded through a pulsed molecular beam valve. Just below the orifice of the pulsed valve, a continuous 1 keV electron beam intersects the gas beam at 90°. Ions are made in the continuum flow region of the jet. Subsequent collisions in the expansion cool the internal degrees of freedom of the ions. Varying degrees of cooling of the vibrational modes can be achieved by changing the carrier gas.

In these experiments, to make CN^- , a mixture of 3% HCN, 8% NF_3 seeded in N_2 is expanded through the pulsed valve. CN^- is produced in the jet by the following reactions:



To produce NCO^- and NCS^- , a few drops of benzyl isocyanate or benzyl thioisocyanate, respectively, are dropped into the valve, and 3 atm of He or a 40% CF_4/He mix, is expanded through the "wet" valve. NCO^- and NCS^- are produced by dissociative attachment of an electron to PhCH_2NCO or PhCH_2NCS . The CF_4/He mix is found to give far superior cooling for vibrational modes of the NCS^- ion.

The ions are perpendicularly extracted into a time-of-flight mass spectrometer of Wiley–McLaren design.²³ The mass-selected ion of interest is photodetached using a pulsed Nd:YAG laser that propagates perpendicular to the ion beam. In these experiments, the fourth (266 nm, 4.657 eV) or fifth (213 nm, 5.822 eV) harmonic of the Nd:YAG laser is used. Photoelectrons ejected from the mass selected ion are detected at the end of a 1 m field-free flight tube which is orthogonal to the laser and ion beams. The energy of the detached electrons is determined by time of flight. The energy resolution is 8 meV for electrons with 0.65 eV of kinetic energy and degrades as $E^{3/2}$ for higher kinetic energies. The polarization of the laser can be adjusted by means of a half-wave plate such that the angle θ between the electric vector of the laser radiation and the direction of electron detection may be sampled. Adjustment of the laser polarization to the magic angle ($\theta=55^\circ$) can be used to eliminate the photoelectron angular anisotropy term.²⁴

Due to the high photon energy employed, any scattered light will release electrons from metal surfaces inside the chamber. This effect is minimized by electron and laser baffles but, even so, at 213 nm the background level is sufficiently high that the background signal must be subtracted from the data. As the kinetic energy distribution of the background photoelectrons is smooth and does not change from day to day, a smooth function is fitted to the background, scaled and subtracted from the experimental spectrum. This subtraction procedure has been followed for the 213 nm photoelectron spectrum of CN^- here.

The calibration procedure used in these spectra is worthy of some discussion. In the photoelectron spectrum of A^- at photon energy $h\nu$, the electron kinetic energy of each peak is determined by

$$eKE = h\nu - EA(A) - E_i(A) + E_i(A^-), \quad (1)$$

where $EA(A)$ is the electron affinity of A (or, equivalently, the electron binding energy of A^-), and $E_i(A)$ and $E_i(A^-)$ are the internal energies of A and A^- for that transition. Ideally, for calibration purposes, the electron affinity and the internal energies of the calibrant species should be extremely well known. At 266 nm the electron kinetic energy scale is calibrated using photoelectron spectra of the atomic ions F^- , Cl^- , Br^- , and I^- , for which the corresponding neutral electron affinities (3.401 190, 3.612 69, 3.363 590, and 3.059 1 eV, respectively²⁵) and neutral atom spin-orbit splittings (0.050 10,²⁶ 0.109 40,²⁷ 0.456 9,²⁶ and 0.942 68 eV,²⁶ respectively) are known to good precision. Each calibrant ion gives two narrow peaks in the photoelectron spectrum,²⁸ and these atomic lines cover the range of electron kinetic energies (0.65–1.60 eV) appropriate for photodetachment at 266 nm. At this wavelength, we can access the ground electronic states of CN, NCO, and NCS, and can therefore accurately determine their electron affinities.

The calibration proceeds as follows: the recorded flight times, t , for each calibrant line are fitted to the following form:

$$t = t_0 + \sqrt{\frac{m_e l^2}{2}} \cdot \frac{1}{\sqrt{E_{\text{lab}}}} + \frac{\gamma}{E_{\text{lab}}}, \quad (2)$$

where m_e is the electronic mass and E_{lab} is the expected electron kinetic energy in the laboratory frame of reference. Using the eight or more calibrant lines, the offset t_0 , the effective flight length l , and the quadratic correction factor γ are determined by least squares. For 266 nm, a linear calibration of the energy scale ($\gamma=0$) is generally sufficient. Using these constants that define the electron energy scale, the flight times for the spectrum of interest are converted to electron kinetic energies; this conversion procedure includes a small center-of-mass correction to the energy.²²

The situation at 213 nm is less auspicious. For this photon energy the halide lines are clustered near electron kinetic energies of 2 eV or above. There are no other atomic negative ions with higher electron binding energies so it is necessary to go to a molecular calibrant ion. One of our motivations for studying CN^- was to obtain calibration points for 213 nm at lower electron kinetic energies. This can be done using the transitions from CN^- to the first excited electronic state of CN, the $A^2\Pi$ state, which lies 0.83 eV above the $X^2\Sigma^+$ ground state. This, of course, requires the accurate value for $EA(\text{CN})$ determined at 266 nm. Thus the results presented in the next section will allow us to better calibrate future spectra at 213 nm. We note here that to fit the electron kinetic energy scale at 213 nm over the entire range covered by the halide and cyanide transitions, the quadratic scale compression factor, γ , must be included. This calibration fit then reproduces all lines to within the measured time-of-flight uncertainties for all

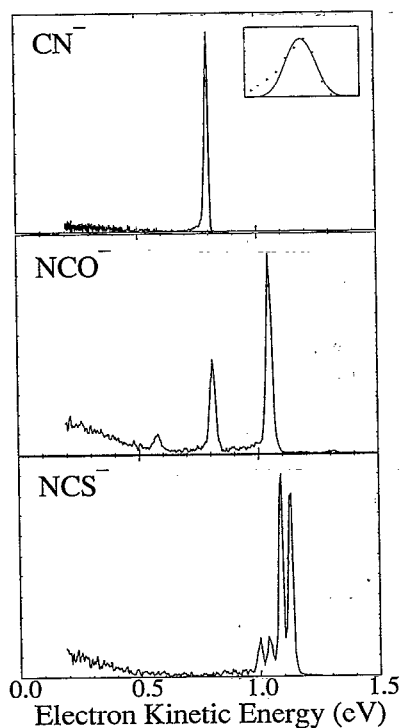


FIG. 1. Photoelectron spectra of (top) CN^- , (middle) NCO^- , and (bottom) NCS^- with 266 nm (4.657 eV) laser radiation. The polarization of laser with respect to the electron collection direction is parallel ($\theta=0^\circ$) for CN^- , magic angle ($\theta=55^\circ$) for NCO^- , and perpendicular ($\theta=90^\circ$) for NCS^- . The experimental spectra have been smoothed by convolution with a 5 meV full-width at half-maximum Gaussian. The inset of the CN^- photoelectron spectrum shows a rotational contour simulation of the $\text{CNX}(^2\Sigma^+) \leftarrow \text{CN}^-X(^1\Sigma^+)$ transition assuming an \bar{n} ion rotational temperature of 200 K (solid line); the experimental data points are indicated by circles. Rotational constants used in the simulation: $B_0'' = 1.875 \text{ cm}^{-1}$, $B_0' = 1.891 \text{ cm}^{-1}$, $D_0'' = -6.202 \times 10^{-6} \text{ cm}^{-1}$, $D_0' = -6.393 \times 10^{-6} \text{ cm}^{-1}$. Refs. 1 and 7.

points.²⁹ The inclusion of a quadratic term in the calibration is similar to that employed on negative ion photoelectron instruments in the Lineberger³⁰ and Ellison³¹ groups. Our conversion scheme from time of flight to electron kinetic energy is analogous to that used on the multiphoton ionization photoelectron spectrometer described by Anderson *et al.*³²

III. RESULTS

The 266 nm photoelectron spectra of the three molecular ions are shown in Fig. 1. The NCO^- spectrum was recorded using the laser polarized at the magic angle ($\theta=55^\circ$) because a change in relative intensities across the band was noticed as a function of laser polarization. For NCS^- and CN^- , although there is sizeable change in absolute counts recorded with the two extreme laser polarizations, the band profile did not change, so spectra were recorded with polarization chosen to maximize signal/noise. This was with $\theta=0^\circ$ for CN^- and $\theta=90^\circ$ for NCS^- . Figure 2 shows the 213 nm photoelectron spectrum of CN^- with the polarization of the laser perpendicular ($\theta=90^\circ$) to the electron collection direction.

The spectra in Fig. 1 are all relatively simple. Photo-

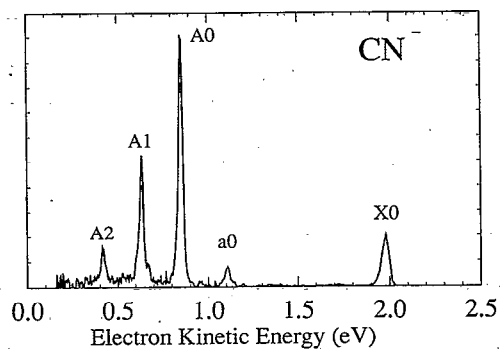


FIG. 2. Photoelectron spectrum of CN^- with 213 nm (5.822 eV) laser radiation. The polarization of the laser is perpendicular ($\theta=90^\circ$) to electron detection direction.

detachment of each ion leads to very little vibrational excitation in the corresponding neutral. The CN^- 266 nm spectrum shows only a single peak, the 0-0 transition, indicating virtually no geometry change between CN^- and the $X^2\Sigma^+$ ground state of CN. In the 213 nm spectrum (Fig. 2), in addition to the X state transition, a more extended progression (peaks A0-A2) in the vibrational levels of the $A^2\Pi$ state is observed. Thus, according to the Franck-Condon principle, there is a somewhat larger geometry change for this anion \rightarrow neutral transition. Since the vibrational spacings and the energy of the electronic origin in the $\text{CN } A^2\Pi$ state are known,¹ peaks A1 and A2 can be used in addition to A0 to calibrate the electron energy scale at 213 nm. The only new spectroscopic feature in Fig. 2 is peak a0. This is a hot band originating from the $v=1$ level of the anion. This spectrum was recorded under source conditions which increased the vibrational temperature of the anions; in other spectra (not shown), this feature can be eliminated. Observation of the hot band is desirable since it represents the first gas phase measurement of the CN^- vibrational fundamental frequency, $2035 \pm 40 \text{ cm}^{-1}$.

The NCO^- photoelectron spectrum shows a short progression in the ν_3 "antisymmetric stretch" mode of the $\text{NCO } X^2\Pi$ state (Fig. 1). Each peak consists of overlapping transitions to the two spin-orbit components of NCO ($A_{000} = -95.6 \text{ cm}^{-1}$).³³ For the $\text{NCS } X^2\Pi$ state, the spin-orbit splitting is much larger ($A_{000} = -323.4 \text{ cm}^{-1}$),³⁴ and transitions to the individual fine structure components are resolved. The spacing between the doublets is close to the ν_3 (C-S stretch) fundamental in NCS . However, a more detailed comparison of the observed peak positions and the term values derived from extensive optical measurements³³ reveals some discrepancies. This is discussed in more detail when we attempt to simulate the NCS^- photoelectron spectrum.

The widths of the observed peaks ($\sim 28 \text{ meV}$ for NCO^- , $\sim 21 \text{ meV}$ for NCS^- , and $\sim 16 \text{ meV}$ for CN^- , 266 nm) are larger than that due the instrumental resolution alone. In the case of NCO , the extra width is due to the unresolved spin-orbit splitting. For the remainder, the peak width is due to sequence bands and the underlying rotational contour for the transition.

TABLE I. Electron affinities of radicals studied in this work.^a

	Raw EA ^b	Correction to peak centroid ^c	Sequence band correction ^d	Space charge correction ^e	Spin-orbit correction ^f	Rotational correction ^g	Final EA ^h
CN	3.860±0.003	+0.003±0.001	0.000±0.000	+0.001±0.001	none	-0.002±0.002	3.862±0.004
NCO	3.615±0.004	-0.005±0.001	+0.002±0.001	+0.003±0.001	-0.006±0.001	0.000±0.002	3.609±0.005
NCS	3.531±0.004	0.000±0.001	+0.002±0.001	+0.004±0.001	none	0.000±0.002	3.537±0.005

^aAll energies in eV.

^bFrom the maximum in 0-0 peak, includes uncertainty in calibration.

^cDifference between weighted peak center and highest point.

^dFrom Franck-Condon simulation.

^eEstimated from halide ion corrections.

^fUnresolved spin-orbit separation, if applicable.

^gEstimated from rotational contour simulation (see the text).

^hCorrected adiabatic electron affinity.

IV. ANALYSIS AND DISCUSSION

A. Electron affinities

The electron affinities for the three radicals can be determined from the 266 nm spectra shown in Fig. 1. The adiabatic electron affinity is estimated as follows. The electron kinetic energy at the peak center of the assigned origin [$E_i(A) = E_i(A^-) = 0.0$, see Eq. (1)] yields the raw electron affinity via

$$EA = h\nu - eKE, \quad (3)$$

where $h\nu$ is 4.657 eV for 266 nm. Corrections are made for the spin-orbit splitting (if appropriate), sequence bands, and any shift between the center of the rotational contour and the rotationless origin. Another factor to be considered in deriving accurate electron affinities is the effect of Coulomb repulsion of the remaining ion charge cloud on the ejected electrons. The interaction of the undetached ion packet with the electron causes the kinetic energy of the departing electron to be increased slightly. We correct for this effect by determining the magnitude of this shift for an atomic ion of similar mass, for the same ion density. Values for all of these corrections are listed in Table I. As can be seen, the magnitude of this latter "space charge" effect is fairly small.

The rotational correction is calculated by simulating the expected rotational contour^{35,36} using the known rotational constants for each molecule and assuming a simple s -wave detachment model developed by Fano³⁷ and Walker.³⁸ This is an approximation; an s -wave model is not strictly appropriate here, since the electron kinetic energies are on the order of 1 eV. Using an anion rotational temperature of 200 ± 50 K, the rotational contour, when convoluted with the instrumental resolution function, matches the experimental line shape, and the (small) correction between peak maximum and rotationless origin for the transition may be estimated. It turns out for all these systems that the correction is smaller than the error bars for the correction process, which nevertheless are propagated into the final uncertainty in the electron affinity. The rotational contour simulation for the photoelectron band to the CN ground state is shown in the inset of Fig. 1. The possibility of broadening of the origin peak in the CN⁻ 266 nm photoelectron spectrum due to the $1 \leftarrow 1$ sequence band

has been checked for; the simulated profile does not change even for vibrational temperatures as large as 1400 K. The final electron affinities derived from this work appear in the final column of Table I.

Let us compare our electron affinity determinations with those currently in the literature. The reported CN electron affinity of Klein *et al.*⁸ obtained via laser optogalvanic spectroscopy is slightly lower than our measurement, and both measurements lie outside the range of their mutual error bars. Klein reports $EA(\text{CN}) = 3.821 \pm 0.004$ eV,⁸ whereas we deduce $EA(\text{CN}) = 3.862 \pm 0.004$ eV from the 266 nm spectrum. We have repeated this measurement several times with independent calibrations, and are therefore confident in our value. To resolve the discrepancy between these two measurements we attempted to measure the total photodetachment cross section on a different apparatus,³⁹ with a tunable dye laser. Such an experiment is much more akin to the optogalvanic experiment, and should provide an independent test. However, in contrast to Klein's experiment, we mass select the CN⁻ before irradiation. This experiment confirmed that the threshold for CN⁻ photodetachment occurs to the blue of Klein's reported threshold; our total detachment cross section rises at 321.1 ± 0.3 nm (3.862 eV) compared to 324.4 nm (3.821 eV). One possible explanation of this discrepancy is that Klein *et al.*, who only observed the 324.4 nm threshold when using BrCN as their source of ions, were actually observing the threshold for the channel $\text{Br}(^2P_{1/2}) \leftarrow \text{Br}^-$, which occurs at 3.8205 eV.^{25,26} Indeed the authors noted a strong slowly rising background due to the $\text{Br}(^2P_{3/2}) \leftarrow \text{Br}^-$ transition throughout the wavelength region they investigated.

Our reported values for the electron affinity of NCO and NCS are in excellent agreement with some recent theoretical determinations, but in varying agreement with experimental estimates. For NCO, there have been numerous experimental determinations of the electron affinity. Brauman and co-workers⁴⁰ observed that NCO has a higher EA than fluorine [3.401 eV (Ref. 25)]. Oster and Illenberger estimate $EA(\text{NCO}) = 3.8 \pm 0.2$ eV based their observed 0 eV appearance potential of NCO⁻ and SF₅⁻ from low energy electron attachment to SF₅NCO,⁴¹ although this is only an upper limit if the appearance energies are less than

0 eV. Dillard and Franklin calculated $\text{EA}(\text{NCO}) = 1.56$ eV from the heats of formation of NCO and NCO^- measured in their ion-molecule experiments,¹⁴ but the heats of formation found in this work appear to be inconsistent with currently accepted values. Wight and Beauchamp calculated a value of 3.62 ± 0.2 eV from their measured NCO^- proton affinity using literature heats of formation for $\Delta H_f^0(\text{HNCO})$ and $\Delta H_f^0(\text{NCO})$.⁴² Our direct measurement of the adiabatic electron affinity is consistent with the measurements of both Brauman and Oster, and also with Wight and Beauchamp's derived value. As discussed in Sec. I, previous direct measurements of the NCS electron affinity,¹² in contrast, appear to be incorrect. Our value of 3.537 ± 0.005 eV, however, is in agreement with Dillard's derived value of 3.51 eV.¹⁴

The theoretical values for the adiabatic electron affinities of Koch and Frenking, 3.71 eV for NCO and 3.45 eV for NCS ,¹³ are in good agreement (better than 0.1 eV) with our observed values. These calculated electron affinities are zero-point corrected MP2/6-31+G* energy differences between the optimized ion and neutral structures. Baker *et al.* have presented an exhaustive comparison of *ab initio* estimates of electron affinities for several molecular systems including NCO .^{43(a)} An interesting conclusion of that study was that the use of a simple MP2/6-31+G* scheme for calculating the energy difference between ion and neutral was among the most effective methods for estimating the adiabatic EA, with the caveat that spin contamination in the unrestricted (UHF) radical wave function should be small (as is the case for NCO). This explains the success of Koch's calculations, and we have ourselves found that a MP2/6-31+G** model reliably yields excellent EA's in our own calculations when we compare to other experimental measurements in our laboratory. This is certainly an encouraging result for *ab initio* theory which has traditionally viewed negative ions as one of the hardest classes of molecules to describe correctly.

It appears that all three ions studied here have very similar electron binding energies. This would lead one to suspect that the extra electron would be closely associated with the CN part of the molecule. The considerably larger electron affinities of NCO and NCS relative to OH and SH (1.828, 2.314 eV, respectively²⁵) seem to support this, since, in OH^- and SH^- , the electron is localized on the oxygen and sulfur atoms. However, the HOMO (of π symmetry) for NCO^- has amplitude over all three atoms, not just the CN group, as is shown in Fig. 3. This suggests that the extra electron is actually somewhat delocalized just as for N_3^- [$\text{EA}(\text{N}_3) = 2.68$ eV (Ref. 39)]. The HOMO in NCS^- is also shown in Fig. 3. It appears more localized than the HOMO in NCO^- , but actually has more amplitude on the sulfur end of the molecule than on the CN group. This is consistent with Ramsay's explanation for the large spin-orbit splitting in $X^2\Pi$ NCS radical (323 cm^{-1}) which he attributed to the valence structure that has the unpaired electron localized on the sulfur atom dominating the electronic description of this radical.⁴⁴ The replacement of an oxygen atom by a sulfur atom usually raises the electron affinity of a molecule, but the observation that

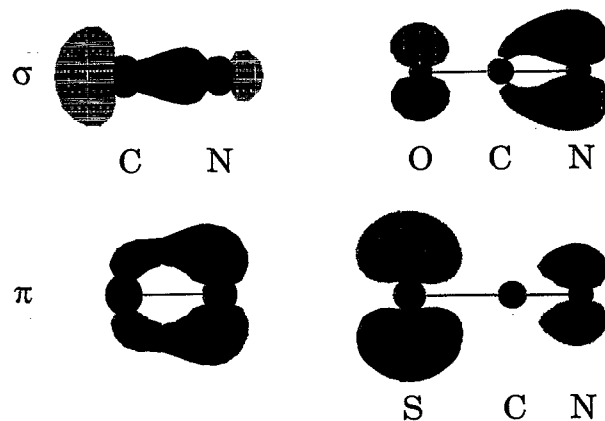


FIG. 3. The highest σ and π molecular orbitals for CN^- , and the highest occupied molecular orbital (HOMO) for each of the NCO^- and NCS^- anions. These are the SCF molecular orbitals computed at the MP2/6-31+G* optimized geometry for each ion. Photodetachment (removal) of an electron from each of these orbitals yields the ground electronic state of the respective neutral radical, except photodetachment from the CN^- π orbital which yields the $\text{CN}(A^2\Pi)$ excited state.

NCO and NCS have similar electron affinities suggests this effect is approximately canceled by the more extensive electron delocalization in NCO^- than in NCS^- . Overall, the electron affinities appear to be determined by the interaction of electron delocalization and electronegativities of various chromophores in the molecule.

B. Derived thermochemical quantities

With a precise estimate of the NCO and NCS electron affinities, we may critically review some related thermochemical quantities. Shobatake⁴⁵ has recently reported the threshold for photodissociation of HNCO



to be $\lambda = 162 \pm 1$ nm. This implies the bond dissociation energy to the \tilde{A} state of NCO , $D^A(\text{H}-\text{NCO}) = 7.65$ eV.⁴⁵ As the T_0 for the \tilde{A} state is well known at 2.82 eV,³⁴ these data together yield a bond dissociation energy, $D_0(\text{H}-\text{NCO}) \leq 111.4 \pm 1$ kcal/mol. Using the ionization potential of hydrogen and our electron affinity for NCO , we calculate $D_0(\text{H}^+-\text{NCO}^-) \leq 341.9 \pm 1$ kcal/mol, and a bond enthalpy $DH_{298}(\text{H}^+-\text{NCO}^-) = 343.2 \pm 1$ kcal/mol. Wight and Beauchamp observed $DH_{298}(\text{H}^+-\text{NCO}^-) = 344.7 \pm 2$ kcal/mol by the proton abstraction reaction of HCO_2^- with HNCO in an ion cyclotron resonance (ICR) machine. Their heterolytic bond dissociation enthalpy is evaluated by comparison to that for formic acid, HCO_2H . The homolytic and heterolytic bond dissociation thermochemistry therefore appears to be consistent. $\Delta H_f^0(\text{NCO}^-)$ may also be re-evaluated from the recent direct determination of the heat of formation of neutral NCO in our laboratory,⁴⁶ $\Delta H_f(\text{NCO}, g, 0 \text{ K}) = +30.4 \pm 1$ kcal/mol, and the electron affinity reported here. Adopting the "ion convention" for ionic heats of formation,¹¹ $\Delta H_f(\text{NCO}^-, g, 0 \text{ K}) = -52.8 \pm 1$ kcal/mol. Using the frequencies in Table II, we estimate $\Delta H_f^0(\text{NCO}^-)$ at 298 K to be unchanged at -52.8 kcal/mol.

TABLE II. Spectroscopic data used in simulation of NCO⁻ and NCS⁻ photoelectron spectra. All values in cm⁻¹.

Mode	A_{000}	ν_1		ν_2		ν_3	
		ω'_1	χ_{11}	ω'_2	χ_{22}	ω'_3	χ_{33}
NCO ⁻	...	1233 ^a	-3.0 ^b	625 ^a	0	2148 ^c	-12.0 ^b
NCO	-95.6 ^d	1279 ^c	-3.0 ^f	535 ^e	0	1951 ^d	-15.0 ^d
NCS ⁻	...	2065 ^h	0.0	469 ⁱ	0	745 ^j	0.0
NCS	-323.4 ^k	1942 ^k	0.0	376 ^l	0	735 ^l	0.0

^aFrom NCO⁻ in CsI matrix. Refs. 15, 16, and 17.

^bFrom NCO⁻ in KI matrix. Ref. 17.

^cFrom gas phase ν_3 fundamental (Ref. 19) and matrix χ_{33} from Ref. 17.

^dReference 34.

^eDerived from NCO gas phase fundamental (Ref. 59) and CO₂⁺ χ_{11} (Ref. 60).

^fFrom CO₂⁺(² Π_g), Ref. 60.

^gReference 61.

^hFundamental in gas phase, Ref. 20.

ⁱNCS⁻ fundamental in CsI matrix, Ref. 18.

^jFundamental in CsI matrix (Ref. 18) and verified as gas phase value by hot band in photoelectron spectrum.

^kReference 33.

^lHarmonic deperturbed analysis of Ref. 33. See the text for details.

For the thermochemical cycles involving NCS⁻, the energy for the HNCS homolytic bond dissociation is less well defined than the heterolytic bond dissociation. We may thus use our electron affinity with the $DH_{298}(\text{H}^+ - \text{NCS}^-)$ of Bierbaum *et al.*⁴⁷ and the ionization potential of the H atom to deduce $DH_{298}(\text{H}-\text{NCS}) = 96 \pm 6$ kcal/mol. The temperature dependence of the electron affinity and ionization potential have been ignored here. The homolytic bond dissociation energy calculated here is considerably lower than the 111 ± 1 kcal/mol literature value listed in Lias.¹¹ However, this value for $DH_{298}(\text{H}-\text{NCS})$ was derived from Page's comparison of the "apparent" electron affinities of NCS measured with the magnetron technique using HNCS and (NCS)₂ as precursors.¹² It is becoming fairly clear that this technique relies on rather too many other thermochemical assumptions to be trusted. Surprisingly, Lias' compilation neglected the more recent work of D'Amario⁴⁸ from which $DH_{298}(\text{H}-\text{NCS})$ could be calculated. D'Amario's derived $\Delta H_f^0(\text{NCS}) = 76.4 \pm 1$ kcal/mol from the photodissociation thresholds of CH₃SCN and CH₃NCS to produce NCS. Using

$$DH_{298}(\text{H}-\text{NCS}) = \Delta H_f^0(\text{NCS}) - \Delta H_f^0(\text{HNCS}) + \Delta H_f^0(\text{H}), \quad (4)$$

$\Delta H_f^0(\text{HNCS}) = +30.6 \pm 0.5$ kcal/mol,¹¹ and $\Delta H_f^0(\text{H}) = +52.1$ kcal/mol,⁴⁹ $DH_{298}(\text{H}-\text{NCS}) = 98.0 \pm 1$ kcal/mol is derived.⁵⁰ Our unambiguous result for the electron affinity of NCS, coupled with Bierbaum's gas phase acidity for HNCS confirms this lower value for $DH_{298}(\text{H}-\text{NCS})$.

C. Simulations

Our goal in this section is to use a simple Franck-Condon model to simulate the photoelectron spectra, allowing us to derive some structural and vibrational parameters for the negative ions. The method employed for

Franck-Condon modeling is due to Hutchisson,⁵¹ and treats each mode as an independent Morse or harmonic oscillator within the normal mode approximation. In addition, we assume that the form of the normal coordinate for a mode changes little between anion and neutral; this is known as the parallel mode approximation. Anion state populations are determined by Boltzmann factors characterized by one (or more) vibrational temperatures.

1. CN⁻

The 266 nm spectrum (Fig. 1) consists of a single peak: CN($X^2\Sigma^+$)($v'=0$) ← CN⁻($v''=0$). The absence of a ($v'=1$) ← ($v''=0$) peak indicates that CN⁻ has a bond length similar to ground state of CN: 1.1718 Å.¹ The 213 nm spectrum (Fig. 2) shows a single peak due to a transition to the X state, as well as a progression due to transitions to the A state of CN. The A state bond length is 1.2223 Å.¹ By simulating the Franck-Condon Factors for transitions to the two states we may bracket the value of R_e in CN⁻.

In the simulations we use the known equilibrium bond lengths, harmonic frequencies and anharmonicities for the X and A states of CN, as well as the spin-orbit coupling parameter of -52.6 cm⁻¹ for CN $A(^2\Pi)$.¹ There is no spin-orbit splitting in the CN ground $X(^2\Sigma^+)$ state. The anion vibration is also treated as a Morse oscillator; the anharmonicity used is that calculated for CN⁻ by Peterson and Woods,⁶ and the harmonic frequency is derived from this anharmonicity and the value of the fundamental observed in our spectrum. We vary only the anion equilibrium bond length and the vibrational temperature until a satisfactory fit to the experimental spectrum is obtained. Franck-Condon factors for transitions to the two electronic states of the neutral are calculated separately. For transitions to the $X(^2\Sigma^+)$ state, values of R_e^{anion} in the range $1.162 \text{ \AA} < R_e^{\text{anion}} < 1.182 \text{ \AA}$ were acceptable in predicting intensity $< 2\%$ in the $v=1-0$ transition, in accord with the absence of this feature in the experimental spectrum; this range is centered on the value of R_e in the ground state of the neutral (1.1718 Å). This result also confirms that the anion bond length is shorter than that in the CN $A(^2\Pi)$ state (1.2333 Å). Figure 4 shows our best fit to the photoelectron band due to transitions to the A state, with $R_e^{\text{anion}}(\text{C}-\text{N}) = 1.1765 \text{ \AA}$. Values of R_e ranging from 1.173 to 1.182 Å gave acceptable fits to the observed intensity distribution, allowing for the uncertainties in experimental peak heights determined from Poisson counting statistics. The experimental observation of two photoelectron bands allows independent determinations of $R_e^{\text{anion}}(\text{C}-\text{N})$. The results are completely consistent; our final estimate of the anion equilibrium bond length is $R_e = 1.177 \pm 0.004 \text{ \AA}$. This result is in excellent agreement with the Peterson and Wood's MP4(SDQ) prediction of $R_e = 1.1772 \text{ \AA}$ and Botschwina's value of $1.1768 \pm 0.001 \text{ \AA}$ calculated with the coupled electron pair approximation (CEPA-1) method.^{6,7}

Let us compare our observed gas phase value of 2035 ± 40 cm⁻¹ for the CN⁻ fundamental frequency with other reported values. The vibrational frequency of the an-

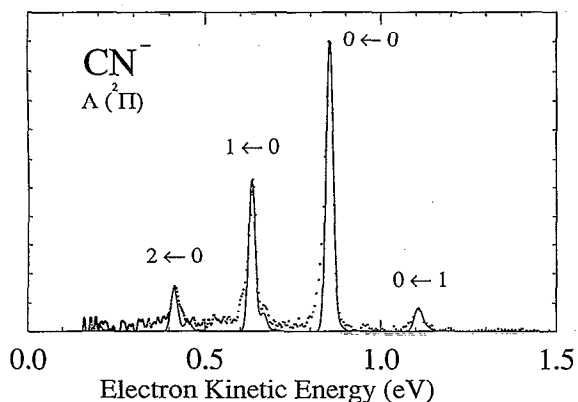


FIG. 4. Franck-Condon simulation for the $\text{CN } A(2\Pi) \leftarrow \text{CN}^- X(1\Sigma^+)$ band. Experimental 213 nm data plotted as points. $R_e^{\text{anion}} = 1.1765 \text{ \AA}$, $T_{\text{vib}} = 1400 \text{ K}$.

ion is 2080 cm^{-1} in aqueous solution and 2076 cm^{-1} in KCN crystal.² Frequencies ranging from 2068 to 2106 cm^{-1} were observed in various CN^- doped alkali-metal halides.³ Mendenhall *et al.* gave $\omega_e = 2125 \pm 6 \text{ cm}^{-1}$ and $\omega_e x_e = 14.2 \pm 0.7 \text{ cm}^{-1}$ for CN^- in KCl, and similar values for CN^- in NaCl and NaBr.³ Sherman and Wilkinson plotted the observed CN^- frequency in these various alkali halides (over 250 measurements) versus the estimated shift due to the matrix, calculated from a lattice perturbation model, and predicted a free space vibrational frequency for CN^- of $2038 \pm 3 \text{ cm}^{-1}$,⁴ in excellent agreement with our measurement. Very recently, Forney *et al.*⁵ isolated CN^- in a neon matrix. The observed fundamental frequency in this inert and nonpolar environment was 2053.1 cm^{-1} . The *ab initio* calculation of Peterson and Woods predicted $\omega_e = 2081.7 \text{ cm}^{-1}$ (and $\omega_e x_e = 13.58 \text{ cm}^{-1}$ which we have used in our fit), giving a fundamental of $2055 \pm 6 \text{ cm}^{-1}$,⁶ Botschwina similarly computed $2052 \pm 6 \text{ cm}^{-1}$ for the anion fundamental.⁷ It appears that the observed value is in reasonable accord with the *ab initio* work, and is, as expected, lower than the reported frequencies in condensed media. This trend is also reported for the C-N stretching frequency in NCO^- and NCS^- .^{4,52} For comparison, the vibrational fundamentals for CN radical in the $X(2\Sigma^+)$ and $A(2\Pi)$ states are 2042.4 and 1787.3 cm^{-1} , respectively.¹

A simple molecular orbital picture of bonding in the CN species would suggest that the neutral has a bond order of 2.5, while the negative ion has a bond order of 3; we thus expect the bond length in the ion to be shorter than that of the radical (1.1718 \AA) and the harmonic frequency to be higher. The A state of CN also has a bond order of 2.5, but it has a longer bond length than the ground state (1.2333 \AA). In fact we find, in agreement with the *ab initio* calculations, that the negative ion has a slightly longer bond length than the ground state of the neutral and a similar or slightly smaller vibrational frequency. Thus in contradiction to the bond order arguments, the bond in CN^- is the same strength or slightly weaker than that in CN radical. It appears that the σ electron removed from the negative

ion is only very weakly bonding and has part lone pair character (see Fig. 3), whereas the π electron removed to form the $A(2\Pi)$ state is strongly bonding. This result is consistent with the photoelectron spectra of N_2 ,⁵³ where ionization to $\text{N}_2^+ X(2\Sigma_g^+)$ gives a very small lengthening of the N-N bond, and a photoelectron band dominated by the 0-0 transition, but ionization to $\text{N}_2^+ A(2\Pi_u)$ gives a much larger bond length change and consequently a longer progression. One additional effect comes into play for negative ions: the extra charge on the negative ion weakens, in the absence of any other effects, the bonding overall because all valence electrons are held less tightly by the nuclear charge relative to the corresponding neutral. These arguments go some way in explaining why CN^- has a longer equilibrium bond length than CN, and the relative vibrational frequencies of the anion and radical X and A states.

2. NCO^-

Both NCO and NCS are known to be linear in neutral and anion ground states. Therefore, photodetachment is expected to excite only the bond stretching normal modes. In fact, only the ν_3 mode is appreciably excited in the NCO^- and NCS^- photoelectron spectrum. The intensity distribution in the ν_3 progression allows us to evaluate the normal coordinate displacement between anion and neutral. From these displacements and the force constant matrix, the individual bond length changes between the neutral and anionic species can be determined. We will employ *ab initio* predictions to guide this process. The literature *ab initio* values have been supplemented by our own computations where appropriate; we have used the GAUSSIAN 90 package for all our calculations.⁵⁴ Because of the larger data set available for NCO, we will describe our simulation for the NCO^- photoelectron spectrum in detail. For NCO, the individual neutral bond lengths have been experimentally determined by comparing the ground state rotational constant for ^{15}NCO , observed in the spectroscopy of the $\tilde{A}^2\Sigma \leftarrow \tilde{X}^2\Pi$ electronic band,²¹ and the rotational constant for ^{14}NCO determined (to higher precision) in the microwave spectrum.^{55,56} This means that we can then use the bond length changes derived from our photoelectron data to extract the two anion bond lengths. These values are then checked for consistency with the anion rotational constant as evaluated by vibration-rotation spectroscopy.¹⁹

The *ab initio* data in Table III^{13,43,57,58} suggest that the difference in equilibrium structure between anion and neutral is that the C-N bond lengthens and the C-O bond contracts on removal of an electron. This is because the HOMO of the anion (from which the electron is detached to form ground state NCO) is C-N bonding and C-O antibonding in character (Fig. 3). Further, the *ab initio* data suggests that the change in equilibrium structure involves very little change in the overall end-to-end length [$R_e(\text{N-O})$]. As the normal modes for this molecule are very close to the symmetric and antisymmetric stretches of CO_2 , these described geometry changes map almost exclusively onto a displacement along the "antisymmetric" normal coordinate, Q_3 , and little change along the "symmetric" stretch, Q_1 . This qualitative description is clearly in

TABLE III. Calculated and observed geometries of NCO^- and NCO .^a

Theory level	NCO^-				NCO			
	$R_e(\text{C-N})/(\text{\AA})$	$R_e(\text{C-O})/(\text{\AA})$	$R_e(\text{N-O})/(\text{\AA})$	$B_e(\text{cm}^{-1})$	$R_e(\text{C-N})/(\text{\AA})$	$R_e(\text{C-O})/(\text{\AA})$	$R_e(\text{N-O})/(\text{\AA})$	$B_e(\text{cm}^{-1})$
HF/6-31G*	1.167	1.215	2.382	0.3971 ^{b,c}	1.212	1.160	2.372	0.4011 ^{b,c}
HF/6-31+G*	1.169	1.214	2.383	0.3968 ^d	1.214	1.159	2.372	0.4011 ^e
MP2/6-31+G*	1.213	1.243	2.456	0.3737 ^d	1.254	1.166	2.411	0.3883 ^e
MRDCI					1.25	1.18	2.43	0.3822 ^f
CASSCF					1.21	1.19	2.40	0.3916 ^g
MR-CI					1.23	1.19	2.41	0.3885 ^g
Experiment	1.17 ^h	1.26 ^h	2.42 ^h	0.3841 ⁱ	1.200 ^j	1.206 ^j	2.406 ^j	0.3895 ^k

^aAll structures linear.^bReference 13.^cReference 43(a).^dReference 43(b).^eThis work.^fReference 57.^gReference 58.^hThese are $R_0 \pm 0.01 \text{\AA}$ derived from Ref. 21 and this work; see the text.ⁱ B_0 from Ref. 19; $B_e = 0.3859 \text{cm}^{-1}$.^j $R_0 \pm 0.008 \text{\AA}$, Ref. 21.^k B_0 from Ref. 56.

good agreement with the progression seen in the ν_3 mode in the experimental spectrum in Fig. 1. Using the data for vibrations of anion and neutral in Table II, a Franck-Condon simulation is performed to fit the observed photoelectron band. The data shown in the table comes entirely from experimental determinations for NCO in the gas phase,^{34,59-61} and for NCO^- mainly from extensive measurements of vibrational frequencies in several alkali halide matrices.¹⁵⁻¹⁷ All three vibrational modes are included in the simulation to model all sequence and hot bands arising from excited anion states. For both the anion and neutral, Morse potentials are used to describe the ν_1 and ν_3 modes and the bending mode is treated as a degenerate harmonic oscillator; the Renner-Teller effect in the neutral radical is neglected. This level of treatment for the bending mode should be sufficient to describe the peak broadening due to sequence bands. In our one-dimensional model there can be no provision for cross anharmonicity terms χ_{ij} . Consequently, the harmonic frequencies, ω'_i , quoted in Table II are effective values given the independent and diagonal treatment of anharmonicity. Thus $\omega'_1 = \omega_1 + \chi_{13}/2 + \chi_{12}$ and $\omega'_3 = \omega_3 + \chi_{13}/2 + \chi_{23}$.¹⁶ The simulation yields a stick spectrum which is then convoluted with our instrumental resolution function,²² and with an 8 meV Gaussian to approximately include the rotational band contour for the transition.

In the fit, all vibrational parameters (anion and neutral) and the spin-orbit coupling constant are treated as fixed; transitions to each of the spin-orbit components of NCO are weighted equally. The Q_3 displacement is the most important variable parameter in the fit. The Q_1 displacement and the temperatures, T_1 , T_2 , and T_3 describing the Boltzmann distribution of anion vibrational states, are also varied. Varying the temperatures will essentially fit the width and line shape of each peak. Finally, the electron kinetic energy for the progression origin is allowed to vary; this essentially allows improved estimation of the electron

affinity and the effect of sequence bands. We use this to evaluate the sequence band correction to the electron affinity (see Table I).

The overall best fit is shown in Fig. 5. The variable parameters are determined as $|\Delta Q_3| = 0.128 \pm 0.008 \text{amu}^{1/2} \text{\AA}$, $T_3 = T_1 = 775 \pm 50 \text{K}$, $T_2 = 600 \pm 50 \text{K}$. The change in the "symmetric" stretch coordinate is limited to be $|\Delta Q_1| \leq 0.04 \text{amu}^{1/2} \text{\AA}$. The position of the 3_1^0 hot band at 1.32 eV is well fit by the ν_3 fundamental from the gas phase work of Saykally *et al.*¹⁹ The intensity of this hot band determines the vibrational temperature, T_3 , describing this ν_3 anion mode; we obtain an improved fit by assuming a higher temperature for the stretching vibrational modes relative to the lower frequency ν_2 bend mode. This is presumably justifiable because the stretching modes are expected to be more strongly excited initially in the dissociative electron attachment reaction used to generate the NCO^- ions. Moreover, the lower frequency bend mode should be cooled more effectively by collisions in the free jet expansion. Overall, the high vibrational temperatures

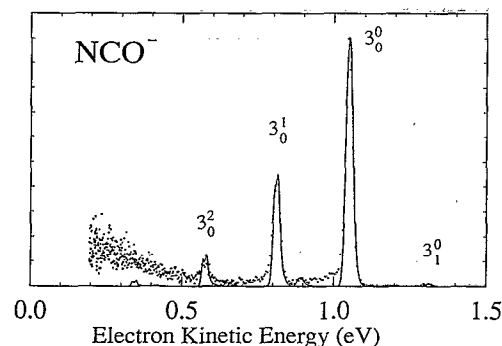


FIG. 5. Simulated photoelectron band for NCO^- photodetachment assuming spectroscopic parameters in Table II. Simulation has anion vibrational temperature set at $T = 775 \text{K}$ for the two stretching modes and $T = 600 \text{K}$ for the bend mode. Experimental data plotted in points.

needed in the fit show that vibrational cooling is fairly poor in the helium expansion.

Jacox has constructed a force constant matrix from infrared observations of all vibrational frequencies of various isotopically substituted forms of NCO in an argon matrix.⁶² From these force constants, we have calculated the bond stretching normal coordinates. When combined with the values of $|\Delta Q_3|$ and $|\Delta Q_1|$ derived from the fit, we may calculate ΔR_{CN} and ΔR_{CO} from anion to neutral.

$$\begin{pmatrix} \Delta R_{\text{CN}} \\ \Delta R_{\text{CO}} \end{pmatrix} = \begin{pmatrix} 0.210 & -0.332 \\ 0.155 & 0.349 \end{pmatrix} \begin{pmatrix} \Delta Q_1 \\ \Delta Q_3 \end{pmatrix}. \quad (5)$$

As we expect the C–O bond to shorten in the neutral and the C–N bond to lengthen, the sign of ΔQ_3 must be negative, but it is not possible to determine the sign of the small ΔQ_1 . Let us then consider three values for ΔQ_1 : +0.04, 0.0, and –0.04. Using $\Delta Q_1 = +0.04$ and $\Delta Q_3 = -0.128$, Eq. (5) yields $\Delta R_{\text{CN}} = 0.050 \text{ \AA}$ and $\Delta R_{\text{CO}} = -0.039 \text{ \AA}$. If we take the R_0 structure for NCO neutral from Misra *et al.* (Table III),²¹ then these displacements yield $R_0(\text{C–N}) = 1.15 \text{ \AA}$ and $R_0(\text{C–O}) = 1.25 \text{ \AA}$ for NCO^- . For $\Delta Q_1 = 0.0$ and $\Delta Q_3 = -0.128$, then $\Delta R_{\text{CN}} = 0.042 \text{ \AA}$ and $\Delta R_{\text{CO}} = -0.045 \text{ \AA}$; resulting in $R_0(\text{C–N}) = 1.16 \text{ \AA}$ and $R_0(\text{C–O}) = 1.25 \text{ \AA}$. Finally if $\Delta Q_1 = -0.04$ and $\Delta Q_3 = -0.128$, then $\Delta R_{\text{CN}} = 0.034 \text{ \AA}$ and $\Delta R_{\text{CO}} = -0.051 \text{ \AA}$; resulting in $R_0(\text{C–N}) = 1.17 \text{ \AA}$ and $R_0(\text{C–O}) = 1.26 \text{ \AA}$ for NCO^- . If we use these values to calculate the rotational constant B_0 for NCO^- , then, by comparing with the high resolution experimental rotational constant, we can determine the sign for ΔQ_1 . For $\Delta Q_1 = +0.04, 0.0,$ and -0.04 the calculated rotational constants are $B_0 = 0.3925, 0.3878,$ and 0.3834 cm^{-1} , respectively. The last of these is closest to the observed $B_0, 0.3841 \text{ cm}^{-1}$,¹⁹ indicating that the sign of ΔQ_1 is negative. The values that best fit the data and agree with Saykally's rotational constant are then $\Delta Q_1 = -0.035 \pm 0.01, \Delta Q_3 = -0.128 \pm 0.008$.

The final result for the anion R_0 bond lengths are shown in Table III. The quoted error bars of $\pm 0.01 \text{ \AA}$ include the uncertainties in the normal coordinate changes in our fit and the error bars in Misra's neutral bond lengths, but not the error in assuming the parallel mode approximation (i.e., the neglect of Duchinsky rotation³⁵) or in Jacox's force constants. Comparing our result to the *ab initio* values shows that the C–N bond length in NCO^- is considerably overestimated at the highest level of theory (MP2). In fact, it appears that all levels of *ab initio* theory shown do not correctly describe the relative bond lengths $R(\text{C–N})$ or $R(\text{C–O})$ in either anion or neutral. It is well known that multiply bonded systems are difficult to describe theoretically and it appears that this system, which has somewhere between a single and double bond between C and O atoms, and between a double and a triple bond between C and N atoms, is certainly a strong test case.

3. NCS^-

The NCS^- photoelectron spectrum has four major peaks; as already noted, these are due to a short progression in the C–S stretch (ν_3) in each of the two spin-orbit

components of the $\text{NCS}^- \tilde{X}^2\Pi$ state. According to this assignment, the four peaks correspond to transitions to the $^2\Pi_{3/2}(000), ^2\Pi_{1/2}(000), ^2\Pi_{3/2}(001),$ and $^2\Pi_{1/2}(001)$ levels of the neutral. However, the spacing of the peak centers from the origin, 0.040, 0.091, and 0.130 eV, differ for the two 3_0^1 transitions from the corresponding term values given by Northrup and Sears³³ (0.040, 0.094, and 0.137 eV) in their laser induced fluorescence/stimulated emission pumping study of NCS. Although these discrepancies are small relative to our resolution, a simulation using Northrup's observed 001 term values cannot fit the observed photoelectron band.

The apparent shift in our peak spacings is probably from Fermi resonances in NCS^- ; Northrup showed these are responsible for extensive mixing of the 020 and 001 states with Π vibronic symmetry. The separation between the $^2\Pi_{3/2}(001)$ and $\mu^2\Pi_{3/2}(020)$ levels is less than 10 meV (80 cm^{-1})—the $^2\Pi_{3/2}(001)$ is higher—as is the separation between the $^2\Pi_{1/2}(001)$ and $\kappa^2\Pi_{1/2}(020)$ levels.³³ (The subscript here refers to P , the projection of the electronic, vibrational, and spin angular momentum along the internuclear axis.⁶³) Close-lying levels with the same value of P can interact via Fermi resonance. In the absence of this effect, the unperturbed 020 levels are expected to have poor Franck–Condon overlap with the NCO^- ground vibrational level. However, because of the Fermi resonance, transitions to the 020 levels can occur with appreciable intensity in the photoelectron spectrum via intensity borrowing from the nearby 001 levels. Thus, we would expect to observe two unresolved doublets in the photoelectron spectrum for the “ 3_0^1 ” peaks. The spacing from the origin of the center of each unresolved doublet would be expected to be the weighted average of the two mixed states making up the doublet. While our resolution is insufficient to resolve these doublets, each 3_0^1 peak in the photoelectron spectrum does lie approximately at the average of Northrup's term values for the strongly interacting $\mu^2\Pi_{3/2}(020)$ and $^2\Pi_{3/2}(001)$ levels, for the $P=3/2$ component and at the average of $\kappa^2\Pi_{1/2}(020)$ and $^2\Pi_{1/2}(001)$ levels for the $P=1/2$ component. Additional evidence for the hypothesis that the 3_0^1 peaks are unresolved doublets is provided by the observation that these peaks around 1.0 eV are broader (25–28 meV) than their respective origin peaks (21 meV) at around 1.11 eV. The contribution to the peak width from instrumental resolution, in contrast, is smaller for peaks at lower electron kinetic energy.

An analogous Franck–Condon simulation can still be performed for the NCS^- spectrum as for NCO^- . However, because of the complications due to the Fermi resonance, which we ignore, and because the observed vibrational progression is very short, we use a simpler, purely harmonic model in this simulation. Because the bending mode is included only for simulation of sequence bands, the ν_2 mode is treated as a degenerate harmonic oscillator for the neutral as well as the ion, without account for the Renner–Teller effect. Northrup and Sears' vibronically deperturbed harmonic frequencies are used for the ν_2 and ν_3 modes (Table II). The deperturbed ω_3 frequency actually matches the observed “ ν_3 ” peak spacing in the photo-

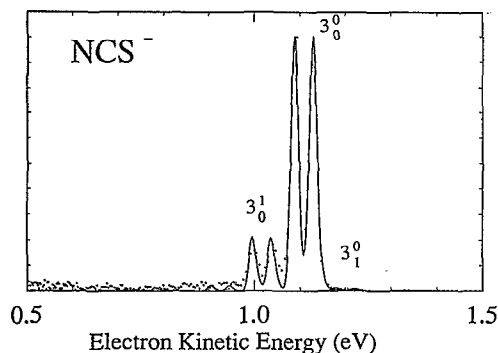


FIG. 6. Simulated photoelectron band for NCS^- photodetachment with anion vibrational temperature set at 350 K, assuming spectroscopic parameters in Table II. Experimental data plotted in points.

electron spectrum. The calculated intensities, however, average the complicated state mixing taking place in the 3_0^1 peaks. For the anion, we also use an entirely harmonic treatment despite the existence of a thorough anharmonic force field derived from alkali halide matrix spectroscopy of NCS^- .¹⁸ This is reasonable because the anion vibrational temperature turns out to be far lower than in NCO^- , so that anion states higher than $v=1$ are not significantly populated. Further, a more complicated treatment does not seem warranted given the simple treatment of the neutral vibrations. The anion ν_1 (C–N stretch) frequency is fixed at the gas phase fundamental observed by Polak *et al.*,²⁰ whereas the ν_2 and ν_3 frequencies are taken from CsI matrix work.¹⁸ Of all the alkali halide matrices, CsI is expected to have the least perturbation on the NCS^- vibrational frequencies, as compared to the gas phase, because it has the largest vacancy sites. Even so, the free ion value for the C–S stretching frequency (ν_3) has been the subject of considerable discussion; it has been suggested that there is still some perturbation caused by the CsI matrix on this “soft” vibration.^{18,52} The position of the 3_1^0 hot band in our photoelectron spectra, particularly where this feature is enhanced in spectra recorded from ions which are formed in a hotter pure helium expansion, is consistent with the ν_3 fundamental observed in cesium iodide. Our

resolution precludes determining the free-ion value with any greater precision.

The variable parameters in the simulation are $|\Delta Q_3|$, the position of the origin, and the vibrational temperature T_{vib} . Here we can adequately fit the spectrum assuming the same temperature for each vibrational degree of freedom. $|\Delta Q_1|$ is constrained to be less than $0.03 \text{ amu}^{1/2} \text{ \AA}$, because little signal is observed at 0.24 eV to lower kinetic energy of the origin, where the 1_0^1 transition is expected, and $|\Delta Q_2|$ must be zero by symmetry. The best fit is shown in Fig. 6, where $T_{\text{vib}}=350 \text{ K}$ and $|\Delta Q_3|=0.13 \text{ amu}^{1/2} \text{ \AA}$. Unlike the NCO radical, only the overall rotational constant for the neutral is known,⁶⁴ and thus the two individual bond lengths are unknown. While there is no force constant matrix available for the radical, one has been constructed for the ion from the alkali halide matrix work.¹⁸ Calculating the normal coordinates for the stretching modes from this force constant matrix, we may again translate our observed ΔQ_3 value into equilibrium bond length changes. In using the anion normal coordinates for this purpose we are once again invoking the parallel mode approximation. By noting that Q_3 corresponds to almost purely C–S shortening/lengthening, that there is no change in Q_1 , and that the rotational constant increases (therefore the overall molecule contracts) from anion to neutral, we can determine that the change in equilibrium bond length between anion and neutral is $\Delta R(\text{C–N})=0.00 \pm 0.01 \text{ \AA}$ and $\Delta R(\text{C–S})=-0.03 \pm 0.01 \text{ \AA}$. Comparing these geometry changes with the *ab initio* data in Table IV,^{13,65} the HF/6–31+G* and HF/6–31G* results are consistent with the changes derived from the Franck–Condon analysis. However, the MP2 results are surprisingly poor; they predict the opposite result, $\Delta R(\text{C–S})>0$ and a substantial shortening in the C–N bond, which is clearly not consistent with the absence of the 1_0^1 peak in the photoelectron spectrum.

V. CONCLUSIONS

We have presented the photoelectron spectra of three pseudohalogen anions. The relatively simple spectra have yielded the electron affinity of CN , NCO , and NCS to a

TABLE IV. Calculated and observed geometries of NCS^- and NCS .^a

Theory level	NCS^-				NCS			
	$R_e(\text{C–N})/(\text{\AA})$	$R_e(\text{C–S})/(\text{\AA})$	$R_e(\text{N–S})/(\text{\AA})$	$B_e(\text{cm}^{-1})$	$R_e(\text{C–N})/(\text{\AA})$	$R_e(\text{C–S})/(\text{\AA})$	$R_e(\text{N–S})/(\text{\AA})$	$B_e(\text{cm}^{-1})$
HF/4–31G*					1.158	1.641	2.799	0.2050 ^b
HF/6–31G*	1.149	1.688	2.837	0.1986 ^c	1.160	1.648	2.808	0.2036 ^c
HF/6–31+G*	1.151	1.686	2.837	0.1987 ^d	1.160	1.649	2.810	0.2033 ^d
CISD/4–31G*					1.154	1.650	2.804	0.2041 ^b
MP2/6–31+G*	1.201	1.659	2.860	0.1970 ^d	1.153	1.672	2.825	0.2007 ^d
Experiment				0.1974 ^e				0.2037 ^f

^aAll structures linear.

^bReference 65.

^cReference 13.

^dThis work.

^e B_e from Ref. 20; $B_0=0.1968 \text{ cm}^{-1}$.

^f B_0 from Ref. 64.

precision of about 5 meV. The electron affinities for all three radicals are now clearly established. Various related thermochemical quantities, including the bond dissociation enthalpy of HNCS, have been derived. The first gas phase determinations of the equilibrium bond length and vibrational frequency for the cyanide ion have also been reported. These data compare very well with high level *ab initio* theory. The results for the 213 nm photoelectron spectrum of CN⁻ provide some useful calibrant lines for negative ion photoelectron spectroscopy at this and shorter laser wavelengths where there have been none hitherto available. A Franck-Condon analysis has yielded the bond lengths in NCO⁻ and the change in geometry for NCS⁻ to NCS. These have been compared to *ab initio* results.

ACKNOWLEDGMENTS

This work has been sponsored by the United States Air Force Office of Scientific Research under Contract Number AFOSR-91-0084. We thank Dr. R. B. Metz for early work on these systems and for performing the total cross section measurements on CN⁻. We would like to thank Professor S. R. Leone for useful discussions on the cyanide results.

- ¹K. P. Huber and G. Herzberg, *Spectra of Diatomic Molecules* Vol. IV (Van Nostrand Reinhold, New York, 1979).
- ²B. M. Chadwick and H. G. M. Edwards, in *Specialist Periodical Report. Molecular Spectroscopy*, Vol. 1, edited by R. F. Barrow, D. A. Long, and D. J. Millen (Chem. Soc., London, 1973), p. 446.
- ³M. Mendenhall, A. Barnes, P. Bunton, R. Haglund, L. Hudson, R. Rosenberg, D. Russell, J. Sarnthein, P. Savundararaj, N. Tolk, and J. Tellinghuisen, *Chem. Phys. Lett.* **147**, 59 (1988).
- ⁴W. F. Sherman and G. R. Wilkinson, in *Vibrational Spectroscopy of Trapped Species*, edited by H. E. Hallam (Wiley, New York, 1973).
- ⁵D. Forney, W. E. Thompson, and M. E. Jacox, *J. Chem. Phys.* **97**, 1664 (1992).
- ⁶K. A. Peterson and R. C. Woods, *J. Chem. Phys.* **87**, 4409 (1987).
- ⁷P. Botschwina, *Chem. Phys. Lett.* **114**, 58 (1985).
- ⁸R. Klein, R. P. McGinnis, and S. R. Leone, *Chem. Phys. Lett.* **100**, 475 (1983).
- ⁹J. Berkowitz, W. A. Chupka, and T. A. Walter, *J. Chem. Phys.* **50**, 1497 (1969).
- ¹⁰M. E. Jacox, *J. Chem. Phys. Ref. Data* **17**, 269 (1988); **19**, 1387 (1990).
- ¹¹S. G. Lias, J. E. Bartmess, J. F. Liebman, J. L. Holmes, R. D. Levin, and W. G. Mallard, *J. Phys. Chem. Ref. Data* **17**, Supp. 1 (1988).
- ¹²R. Napper and F. M. Page, *Trans. Faraday Soc.* **59**, 1086 (1963); F. M. Page, *Adv. Chem. Ser.* **36**, 68 (1972).
- ¹³W. Koch and G. Frenking, *J. Phys. Chem.* **91**, 49 (1987).
- ¹⁴J. G. Dillard and J. L. Franklin, *J. Chem. Phys.* **48**, 2353 (1968).
- ¹⁵W. C. Price, W. F. Sherman, and G. R. Wilkinson, *Proc. R. Soc. London, Ser. A* **255**, 5 (1960).
- ¹⁶V. Schettino and I. C. Hisatsune, *J. Chem. Phys.* **52**, 9 (1970).
- ¹⁷D. F. Smith, J. Overend, J. C. Decius, and D. J. Gordon, *J. Chem. Phys.* **58**, 1636 (1973).
- ¹⁸D. F. Smith, Jr., *J. Mol. Spectrosc.* **57**, 447 (1975).
- ¹⁹M. Grubele, M. Polak, and R. J. Saykally, *J. Chem. Phys.* **86**, 6631 (1987).
- ²⁰M. Polak, M. Grubele, and R. J. Saykally, *J. Chem. Phys.* **87**, 3352 (1987).
- ²¹P. Misra, C. W. Mathews, and D. A. Ramsay, *J. Mol. Spectrosc.* **130**, 419 (1988).
- ²²R. B. Metz, A. Weaver, S. E. Bradforth, T. N. Kitsopoulos, and D. M. Neumark, *J. Phys. Chem.* **94**, 1377 (1990).
- ²³W. C. Wiley and I. H. McLaren, *Rev. Sci. Instrum.* **26**, 1150 (1955).
- ²⁴A. Weaver, D. W. Arnold, S. E. Bradforth, and D. M. Neumark, *J. Chem. Phys.* **94**, 1740 (1991).
- ²⁵T. M. Miller, in *CRC Handbook of Chemistry and Physics*, 72nd ed., edited by D. R. Lide (CRC, Boca Raton, 1991), pp. 10-180.
- ²⁶C. E. Moore, *Atomic Energy Levels*, Vol. I NSRDS-NBS **35** (1971).
- ²⁷S. Baskin and J. O. Stoner, Jr., *Atomic Energy Level and Grotian Diagrams*, Vol. 2 (North Holland, New York, 1978).
- ²⁸A. Weaver, Ph. D. thesis, University of California, Berkeley, 1991.
- ²⁹The fit is then a 3 parameter fit to 12 calibrant data points.
- ³⁰D. Leopold, K. K. Murray, A. Stevens Miller, and W. C. Lineberger, *J. Chem. Phys.* **83**, 4849 (1985).
- ³¹D. C. Cowles, M. J. Travers, J. L. Frueh, and G. B. Ellison, *J. Chem. Phys.* **94**, 3517 (1991).
- ³²S. L. Anderson, L. Goodman, K. Krogh-Jespersen, A. G. Ozkabak, R. N. Zare, and C. Zheng, *J. Chem. Phys.* **82**, 5329 (1985).
- ³³F. J. Northrup and T. J. Sears, *J. Chem. Phys.* **91**, 762 (1989); *Mol. Phys.* **71**, 45 (1990).
- ³⁴F. J. Northrup, M. Wu, and T. J. Sears, *J. Chem. Phys.* **96**, 7218 (1992).
- ³⁵K. Ervin and W. C. Lineberger in *Advances in Gas Phase Ion Chemistry*, Vol. 1, edited by N. G. Adams and L. M. Babcock (JAI, Greenwich, in press).
- ³⁶P. C. Engelking, *J. Phys. Chem.* **90**, 4544 (1986).
- ³⁷A. R. P. Rau and U. Fano, *Phys. Rev. A* **4**, 1751 (1971).
- ³⁸T. E. H. Walker, *Chem. Phys. Lett.* **19**, 493 (1973).
- ³⁹R. E. Continetti, D. R. Cyr, R. B. Metz, and D. M. Neumark, *Chem. Phys. Lett.* **182**, 406 (1991).
- ⁴⁰R. L. Jackson, M. J. Pellerite, and J. I. Brauman, *J. Am. Chem. Soc.* **103**, 1802 (1981).
- ⁴¹T. Oster and E. Illenberger, *Intl. J. Mass Spectrom. Ion Processes* **85**, 125 (1988).
- ⁴²C. A. Wight and J. L. Beauchamp, *J. Phys. Chem.* **84**, 2503 (1980).
- ⁴³(a) J. Baker, R. H. Nobes, and L. Radom, *J. Comp. Chem.* **7**, 349 (1986); (b) W-K Li, J. Baker and L. Radom, *Aust. J. Chem.* **39**, 913 (1986).
- ⁴⁴R. N. Dixon and D. A. Ramsay, *Can. J. Phys.* **46**, 2619 (1968).
- ⁴⁵K. Uno, T. Hikida, A. Hiraya, and K. Shobatake, *Chem. Phys. Lett.* **166**, 475 (1990).
- ⁴⁶D. R. Cyr, R. E. Continetti, R. B. Metz, D. L. Osborn, and D. M. Neumark *J. Chem. Phys.* **97**, 4937 (1992).
- ⁴⁷We use the $\Delta H_{\text{acid}}^{\circ}$ re-evaluated in Ref. 11 from the original data of V. M. Bierbaum, J. J. Grabowski and C. H. DePuy, *J. Phys. Chem.* **88**, 1389 (1984).
- ⁴⁸P. D'Amario, G. di Stefano, M. Lenzi, and A. Mele, *J. Chem. Soc. Faraday Trans. 1* **68**, 940 (1972).
- ⁴⁹M. W. Chase, Jr., C. A. Davies, J. R. Downey, Jr., D. J. Frurip, R. A. McDonald, and A. N. Syverud, *JANAF Thermochemical Tables*, 3rd ed. (American Chemical Society and American Institute of Physics, New York, 1986).
- ⁵⁰M. Lenzi, A. Mele, and M. Paci, *Gazz. Chim. Ital.* **103**, 977 (1973).
- ⁵¹E. Hutchisson, *Phys. Rev.* **36**, 410 (1930); **37**, 45 (1931).
- ⁵²M. L. Polak, Ph. D. thesis, University of California, Berkeley, 1990.
- ⁵³D. W. Turner, C. Baker, A. D. Baker, and C. R. Brundle, *Molecular Photoelectron Spectroscopy* (Wiley, London, 1970), p. 46.
- ⁵⁴M. J. Frisch, M. Head-Gordon, H. B. Schlegel, K. Ragavachari, J. S. Binkley, C. Gonzales, D. J. Defrees, D. J. Fox, R. A. Whiteside, R. Seeger, C. F. Melius, J. Baker, R. L. Martin, L. R. Kahn, J. J. P. Stewart, E. M. Fleuder, S. Topiol, and J. A. Pople, GAUSSIAN 90 (Gaussian Inc., Pittsburgh, 1990).
- ⁵⁵S. Saito and T. Amano, *J. Mol. Spectrosc.* **34**, 383 (1970).
- ⁵⁶K. Kawaguchi, S. Saito, and E. Hirota, *Mol. Phys.* **55**, 341 (1985).
- ⁵⁷M. Peric, B. A. Hess, and R. J. Buenker, *Mol. Phys.* **58**, 1001 (1986).
- ⁵⁸M. H. Alexander and A. Werner (private communication).
- ⁵⁹J. Werner, W. Seebass, K. Koch, R. F. Curl, W. Urban, and J. M. Brown, *Mol. Phys.* **56**, 453 (1985).
- ⁶⁰S. Mrozowski, *Phys. Rev.* **72**, 682 (1947).
- ⁶¹P. S. H. Bolman, J. M. Brown, A. Carrington, I. Kopp, and D. A. Ramsay, *Proc. R. Soc. London Ser. A* **343**, 17 (1975).
- ⁶²D. E. Milligan and M. E. Jacox, *J. Chem. Phys.* **47**, 5157 (1967).
- ⁶³ P is the only good quantum number here. It is defined by $P = |\pm \Omega \pm l|$, where Ω is the projection of the sum of orbital and spin angular momentum on the internuclear axis and l is the vibrational angular momentum.
- ⁶⁴T. Amano and T. Amano, *J. Chem. Phys.* **95** 2275 (1991).
- ⁶⁵I. Tokue, K. Kobayashi, T. Honda, and Y. Ito, *J. Phys. Chem.* **94**, 3485 (1990).